Bioinspiration & Biomimetics

PAPER

Flow visualization and force measurement of the clapping effect in bio-inspired flying robots

RECEIVED
27 October 2020

REVISED
14 September 2021

ACCEPTED FOR PUBLICATION
28 September 2021

PUBLISHED
26 October 2021

Miquel Balta, Dipan Deb and Haithem E Taha*

Department of Mechanical and Aerospace Engineering, University of California, Irvine 5200 Engineering Hall, Irvine, CA 92697-2700, United States of America

* Author to whom any correspondence should be addressed.

E-mail: mbaltama@uci.edu, dipand@uci.edu and hetaha@uci.edu

Keywords: clap and fling, flapping-wing micro-air-vehicles, bio-inspired flying robots, flapping propulsion, flow visualization

Supplementary material for this article is available online

Abstract

In this paper, we perform experimental investigations of the aerodynamic characteristics due to wing clapping in bio-inspired flying robots; i.e., micro-air-vehicles (MAVs) that fly by flapping their wings. For this purpose, four flapping MAV models with different levels of clapping (from no clapping at all to full clapping) are developed. The aerodynamic performance of each model is then tested in terms of the average thrust and power consumption at various flapping frequencies. The results show that clapping enhance both thrust and efficiency. To gain some physical insight into the underlying physics behind this clapping-thrust-enhancement, we perform a smoke flow visualization over the wings of the four models at different instants during the flapping cycle.

1. Introduction

Over the last two decades, flapping-wing micro-air-vehicles (FWMAVs) have received significant attention within the scientific community. In 2005, the defense advance research project agency has opened a contest to develop a nano air vehicle (NAV), which was defined as an autonomous flying machine whose maximum dimension is less than 15 cm, with a very light weight (<10 g) and capable of performing a variety of civil and military applications [1, 2]. These miniature vehicles were meant to be for indoor reconnaissance and surveillance. With the successful development of the NAV hummingbird by Aerovironment, it was shown that hovering and forward flight could be attained through flapping-wing only propulsion [3].

One of the most special micro air vehicles (MAVs) is the flapping-wing type that flies like insects or birds. Flapping insects use unconventional aerodynamic mechanisms (e.g. leading edge vortex (LEV)) to create high lift at ultra-low Reynolds numbers [4–6]. They also exploit unconventional stabilization mechanisms (e.g. vibrational stabilization) to stabilize their bodies during flight and recover from gust disturbances [7–11].

Recently, several research groups have independently developed different unique designs. Harvard engineers [12] designed and built the smallest FWMAV, the Aerovironment nano humming-bird set the standard for the flight performance and control of FWMAVs [13], and TU Delft developed the well-known Delfly family which uses a bi-plane flapping configuration [14, 15]. Inspired by their corresponding biological flyers, FWMAVs usually hover using a horizontal stroke plane [16, 17]. This design allows two degrees of freedom for the wing (assuming rigid): back-and-forth flapping and pitching. However, the stringent size, weight and power constraints typically imposed on the design of FWMAVs urged most of the concepts [16, 18–20] to adopt passive control for the pitching angle. On the other hand, in order to achieve optimal flapping performance, one may have to use active control of the wing pitching angle [21, 22]. Hence, it is of great interest to design actuation mechanisms that not only control the flapping angle [23], but also allow control of the pitching angle using only one drive motor.

Balta *et al* [24] developed a novel active pitching mechanism, which controls both the pitching and flapping angles using only one actuator. This mechanism can achieve a pitching motion profile that is syn-

chronized with the flapping motion, hence improving the performance of the FWMAV. In order to construct an air vehicle with this new flapping mechanism, we modified a flapping drone from the available market, shown in figure 1(a). This flapping drone uses a passive pitching mechanism that powers four wings (two pairs of wings), which clap once during each cycle.

The flapping mechanism of the commercially available flapping drone is neatly manufactured. So, we opt to modify it rather than manufacture a whole new mechanism. The modification procedure is as follows: from a passive mechanism that powers four wings to a passive mechanism that powers two wings, and then to an active mechanism that powers two wings, as shown in figure 1(b). While doing so, we found that the thrust capability considerably decreases when the passive four-wing air vehicle is transformed into the corresponding passive two-wing air vehicle. In other words, an FWMAV with four wings that flies by clapping its wings generates a considerably larger thrust than an FWMAV with two wings having the same frequency and double the stroke angle. It should be noted that this behavior is not intuitive since the generated thrust depends linearly on the number of wings and quadratically on the stroke angle. The unconventional aerodynamics of this phenomenon urged the team to study the thrust generation mechanism due to clapping in more detail, which is the main focus of this paper.

In fact, the clap and fling mechanism has been widely studied over the past few decades. Weis-Fogh was the first to point to lift enhancement in insects and birds due to clap and fling [26, 27], which triggered several research efforts in this direction (e.g. [20, 23, 28, 29]). Sane studied the improvement of flight forces by some mechanisms, such as the wing–wake interaction, at different angles of attack [30]. Tay *et al* investigated the impact of the size on force production [31]. Their explanation of the clap-and-fling/peel mechanism are summarized in figure 2. However, the more recent results of Martin *et al* [32] concluded that such a lift enhancement actually depends on the Reynolds number. Moreover, even when there is a clapping lift enhancement, the strength of such enhancement also depends on the Reynolds number [33], which may highlight the important role of elasticity in this mechanism.

The effect of flexibility on clap and fling motion has also been studied concluding that flexible wings are more effective in generating desirable forces [32, 34, 35], which is intuitively expected. Moreover, it was found that more flexible wings adjust their feathering angle in a way mitigates undesirable phase delay, which leads to an increase of the aerodynamic force [20]. The benefit is also extended to the efficiency, where FWMAVs with flexible wings are proven to passively increase their efficiency, as they store and release elastic energy every cycle [36, 37]. Effects of different aspect ratios and stroke angles have been investigated in the context of vortex dynamics in clapping motion [38].

Mathematical modeling of aerodynamic forces during clap-and-fling in FWMAVs is quite a challenging task due to the associated rich flow physics. The first models [30, 39] focused on studying multiple flight cases and proved that wing–wing and wing–wake interactions provide exceptional lift enhancement beyond steady aerodynamic properties. Percin *et al* [35] have investigated wing kinematics with structural deformation measurement synchronized with force and power consumption. They found out that the wing–wing interaction not only creates favorable flow condition but also influences the aerodynamic forces through changing the effective wing geometry. Moreover, they observed a favorable effect of increasing aspect ratio on the force to power consumption ratio (i.e., efficiency). Armanini *et al* [28] focused on producing a model for the time-resolved aerodynamic forces in the clap-and-fling mechanism. They realized that in order to construct a model that predicts accurately the time-variation of the lift force during clap and fling of the test platform, it is essential to account for the wing–wing interaction (they did it by including a fling circulation factor). Additionally, in their following work on clap-and-peel [40], they were able to decouple the effect of wing–tail interaction and model it separately from the wing's. This addition improved their estimation of the lift force and provided more clarity on the impact of each characteristic of the model.

A comparison between different flight mechanisms in insects, birds and bats, was carried out by Marden [41]. He realized that the majority have the same lift generation during takeoff except for the ones that exploit clap-and-fling, which created about 25% more lift. Later, Cheng and Sun [42] performed a comparative study between full clap and partial clap by numerically solving the Navier–Stokes equations. Based on their analysis of the pressure distribution over the wings, it was concluded that partial clap motion is more practical for insects. It enhances the lift force without negatively impacting their efficiency. Nakata *et al* [20] have investigated the flexible wing aerodynamics of a bio-inspired flapping MAV by combining CFD with wind tunnel measurements. They have showed that using the same model, the four-wings MAV generates twice the lift force of its two-wings counterpart, at body angle larger than 40°. Also, they found that the two-wings MAV with a softer Mylar wings generates more lift forces than the four-wings MAV in case where the body angle was larger than 30°, which shows the paramount role of aeroelasticity in the clap-and-fling mechanism. Additionally, Tay *et al* [31] proved using their quantitative model that even if the flapping wing MAV is reduced to a size of an insect, the x-wing configuration provides two times more lift force than a

Figure 1. Commercial flapping drone and our modified version with an active pitching mechanism. (a) Commercial flapping wing drone [25]. (b) Modified version of the flapping wing air vehicle with an active mechanism (top view).

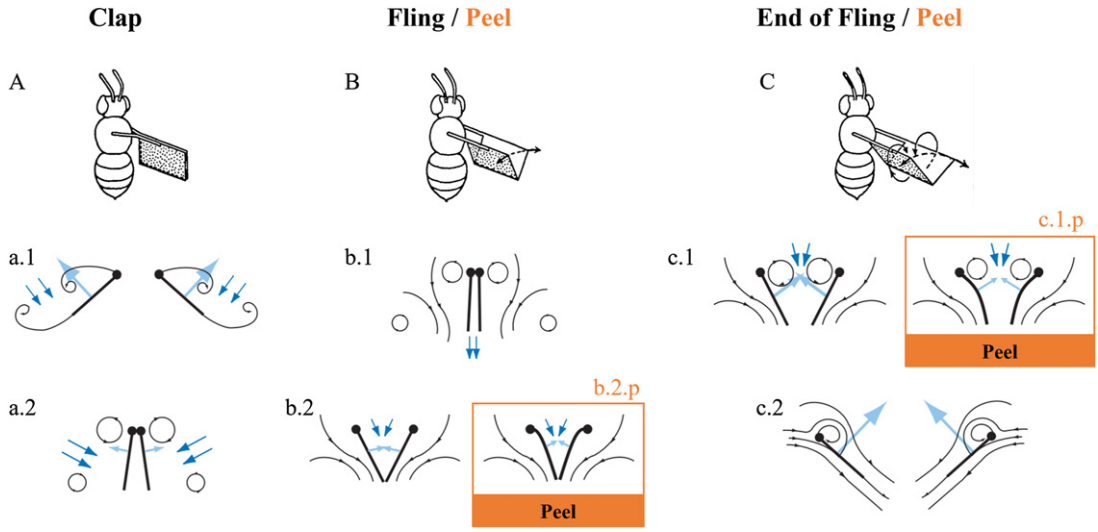

Figure 2. Summary of the clap-and-fling/peel mechanism based on the previous literature. (A), (B), and (C) Reproduced with permission from [26]. (a.1), (a.2), (b.1), (b.2), (c.1), and (c.2) Reproduced with permission from [30]. (b.2.p), and (c.1.p) Reproduced from [31]. © IOP Publishing Ltd. All rights reserved. The flight sequence goes from (A) to (C), or from (a.1) to (c.2).

regular two-wing model. These results were also validated by Nguyen *et al* [43], who found a 44.82% more lift in the four-wings compared to two-wings using an own model similar to the 'DelFly II'. Lehmann *et al* [44] found an increase of lift of 17% when using two computer-controlled rigid wings that were designed to clap-and-fling. This lift enhancement is considerably less than that by the other researchers, reported above, because the wings were significantly more separated on the closing stage. Finally, Jadhav *et al* [29] performed a focused study on the clap portion of the clap-and-fling. Using CFD and PIV, they found that the closer the clap, the higher the lift generated.

These results point to the important role played by closing gap at the end of clapping, which has not been duly studied in the literature using flexible wings (perhaps Cheng and Sun [42] is the most relevant effort that gave some attention to this study). Other research efforts have studied the effect of the gap at the end of the stroke, but did not find a major increase in the vertical force during those moments [45–47]. However, these efforts were using rigid wings, which may point to the importance of flexibility in exploitation of clap and fling, as discussed by Nakata *et al* [20]. Therefore, it urges a more detailed experimental research with proper FWMAV models that are specifically developed for the comparative study.

To assess the effect of full and partial clapping and the aerodynamic mechanism that generates such increase in lift forces, we engineered four FWMAV models with: (i) four wings that fully clap, (ii) four wings that partially clap, (iii) four wings that do not clap, and (iv) two wings. We analyzed the thrust and power characteristics of each FWMAV model at different flapping frequencies. In the light of these force and power measurements, we conducted flow visualization using high-resolution, high-speed camera to obtain physical insights into the reason behind the clapping unsteady lift enhancement mechanism.

2. Experimental setup

The research focus is on analyzing the aerodynamic performance of clap and fling mechanism due to

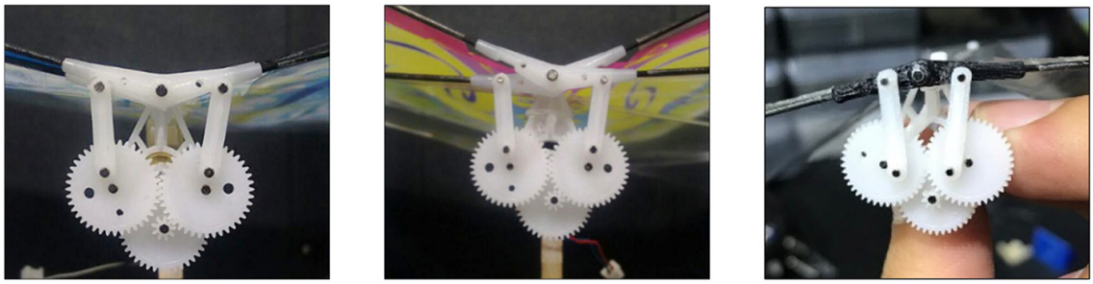

Figure 3. Top view of the mechanisms used in each model of the FWMAV. (a) Model A. (b) Models B and C. (c) Model D.

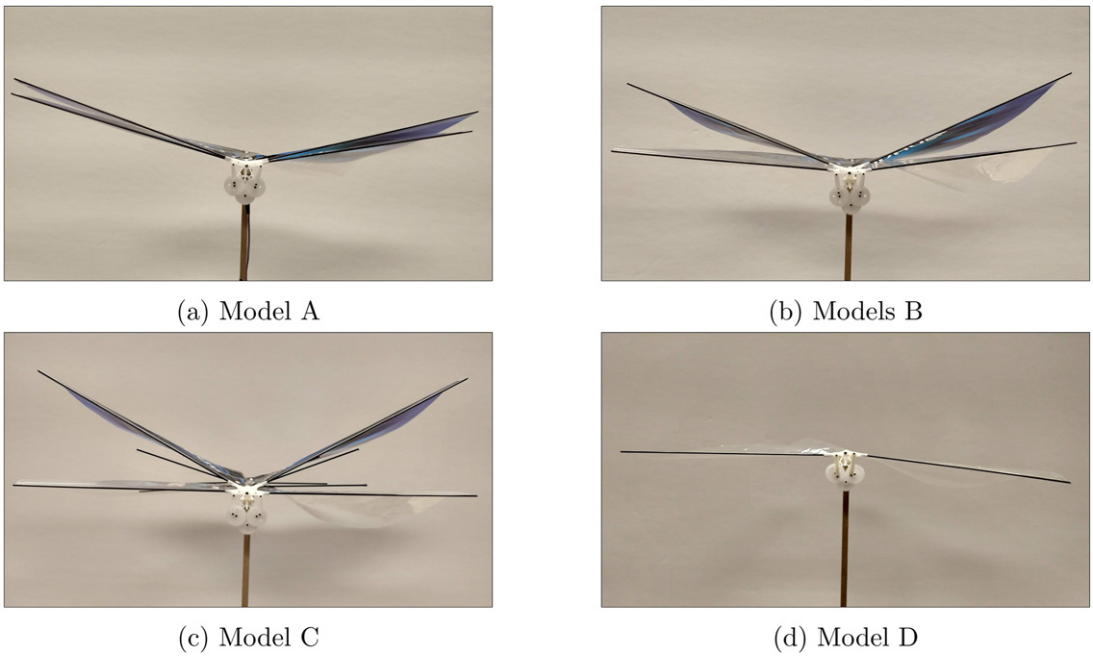

Figure 4. Top view of the four models. (a) Model A. (b) Models B. (c) Model C. (d) Model D.

wing–wing interactions. During the flapping cycle when wings come closer; it is called clapping and when it separates away, that part of the cycle is named as fling. Therefore, we developed four models with different wing configurations (see figures 3–5). The first model (A) has four wings that close and clap completely, the second model (B) has four wings that close and clap partially, the third model (C) has four wings that close partially but do not clap (thanks to the separator placed between the wings, see figure 6), and the fourth model (D) has only two wings, which operates with almost double the stroke angle.

The observation that triggered this study is the considerable difference in aerodynamic behavior between the models B and C, which are almost identical, but the former claps partially and the latter does not clap. Then, by analyzing the two most different systems (models A and D), we can understand the underlying physics behind the boosted performance due to clapping. Comparisons are performed between the four models in terms of the average thrust and power consumption at different flapping frequencies. Additionally, the flow dynamics has been qualitatively captured using a flow visualization setup.

2.1. Characterization of the models

The FWMAVs used in the experiment have the same characteristics expect for the mechanism. As discussed in our previous effort [24], the mechanism is a crank rocker, which transforms a circular motion into an oscillatory one. The first model (A) uses two crank rocker mechanisms where two wings are attached to linkage 4 in the mechanism (see figure 7). Therefore, the wings can clap completely. The second and third models (B and C) have a modified mechanism that only allows the FWMAV to clap partially (see figures 5(b) and (c)). This is achieved by increasing the length of rod 1, which is the base (see figure 7(b)). As for the third model (C), we added four rods on each side to prevent clapping (see figure 6(b)). In the fourth model (D) the linkage 4 is replaced by a similar one that is attached to only one wing, as shown in figure 3(c). All models are equipped with the same

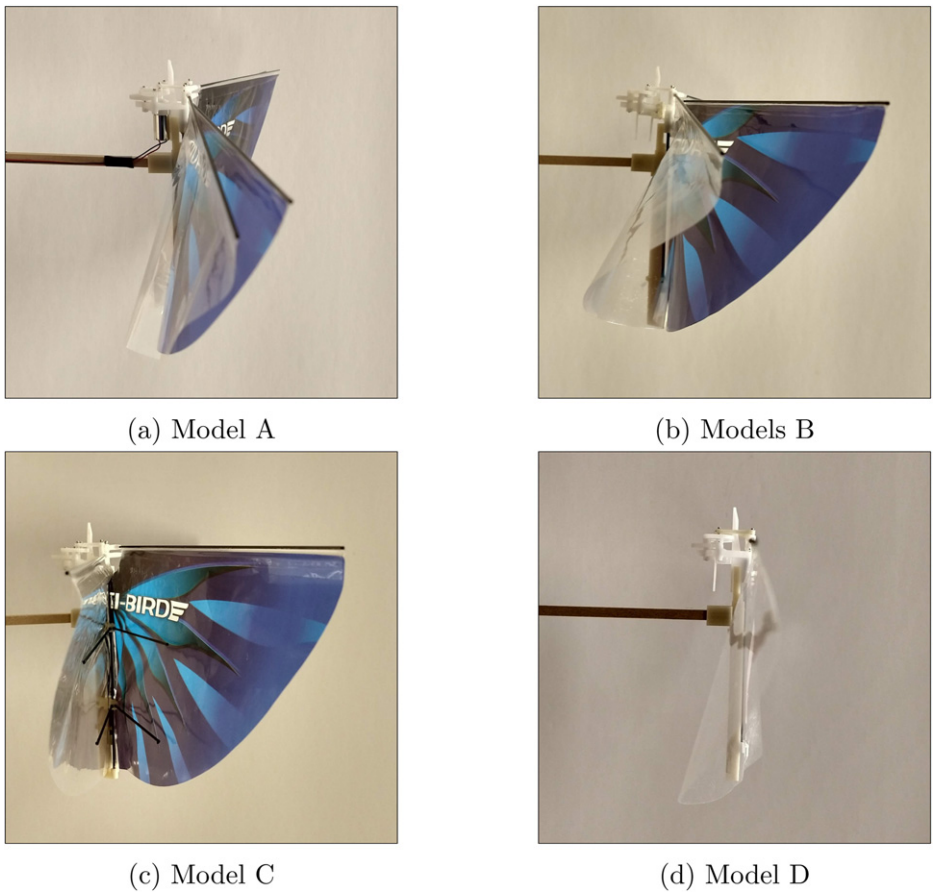

Figure 5. Side view of the four models. (a) Model A. (b) Model B. (c) Model C. (d) Model D.

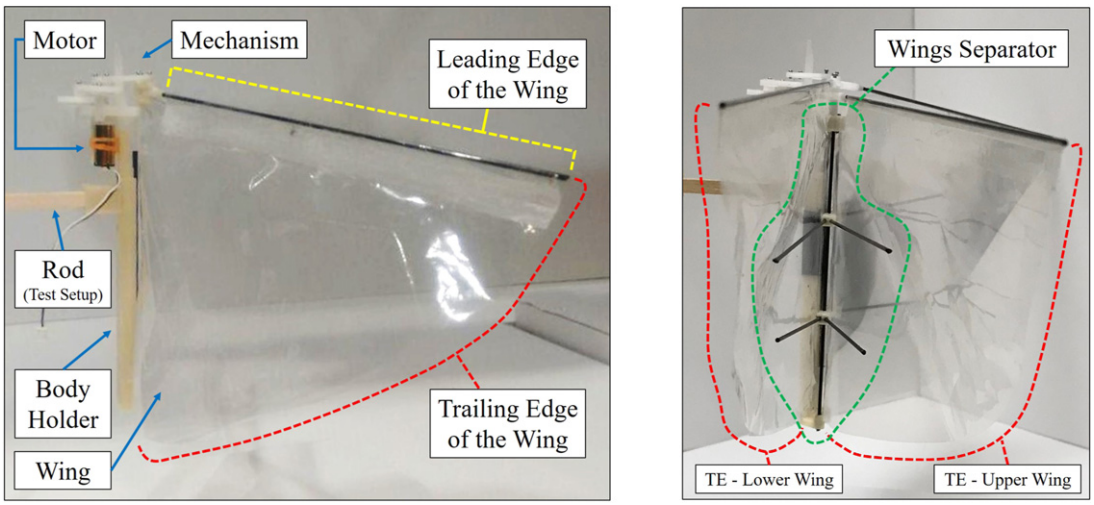

Figure 6. Side views of model D and model C, which shows the separator structure used to prevent the wings from clapping. (a) Side view of the model D. (b) Wings separator of the model C.

wings, with span of 28.2 cm and maximum chord of 9.5 cm. The rest of the parameters are shown in table 1.

The stroke angle of the wing is the angle enclosed by the two extreme positions of the wing during the cycle. In the four-winged models (A, B and C), the wings go from 0° to ±35°, which means that the stroke angle of one wing is 35°. On the other hand, in the two-winged model (D), the stroke angle is 60°.

2.2. Averaged thrust and power measurements

The experimental setup consists of a pendulum that has one degree of freedom, with the mass of the pendulum replaced by the FWMAV model, as shown in figure 8. As such, at a given frequency, the steady state

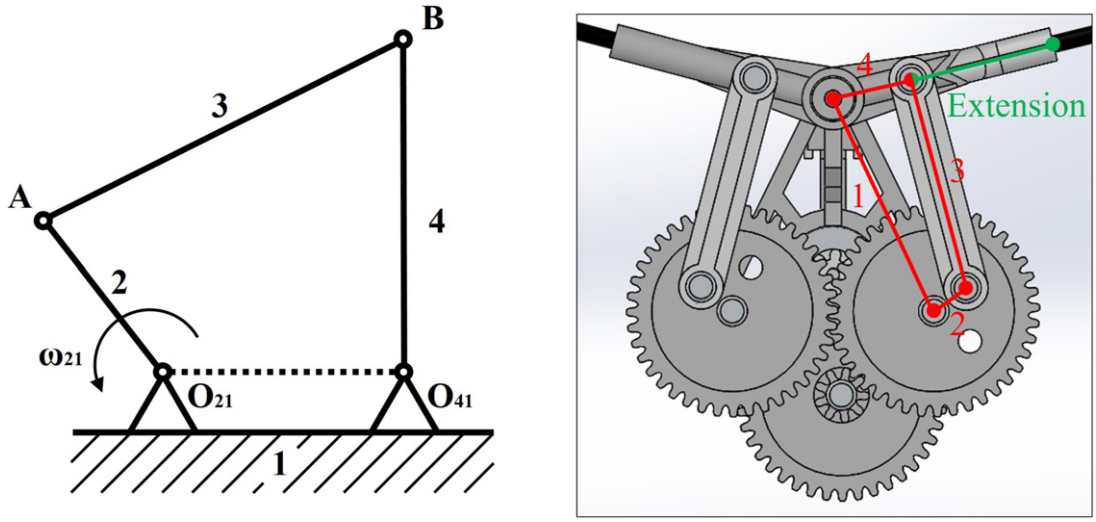

Figure 7. Crank rocker mechanism used in the models of this study. (a) Schematic of the crank rocker mechanism. (b) Crank rocker mechanism from model A.

Table 1. Description and basic properties of each FWMAV used in the research.

FWMAV	Description	Number of wings	Stroke angle	Weight
Model A	FWMAV with four wings and full close/clap	2/side	35°/wing	8.17 gr.
Model B	FWMAV with four wings and partial close/clap	2/side	37°/wing	8.37 gr.
Model C	FWMAV with four wings, partial close and no clap	2/side	37°/wing	9.8 gr.
Model D	FWMAV with two wings	1/side	60°/wing	7.36 gr.

pendulum angle θ is used to estimate the averaged thrust T as:

$$T = \left(m_{\text{FWMAV}} + \frac{1}{2}m_{\text{rod}}\right) g \sin\theta, \qquad (1)$$

where m_{FWMAV}, m_{rod} are the FWMAV and rod masses, respectively. In this test, we also read the provided voltage and current from the power supply to estimate the *total* averaged power consumption. This configuration is preferred over the Harvard Robofly experimental setup (moving along vertical rails) [48] because it allows multiple equilibrium *positions* at different flapping frequencies [9]. Also, it is preferred over a completely static configuration [20, 29, 35, 37, 40, 43] because it allows the FWMAV's body to oscillate around the hovering equilibrium; hence, it accounts for aerodynamic–dynamic interactions [7, 10]—mimicking hover more realistically. Moreover, the same test is repeated without wings to obtain the *mechanical* power consumption of the mechanism at different frequencies. Therefore, the *aerodynamic* power can be obtained from the relation:

$$\text{Aerodynamic Power} + \text{Mechanical Power} = \text{Total Power}. \qquad (2)$$

This aerodynamic power consumption is the main comparison metric used to assess the efficiency of a given model.

2.3. Flow visualization test

The flow visualization test allows us to study the qualitative physics due to the interaction between the wings and the surrounding air. Therefore, we can gain physical insight about the thrust enhancement observed in the average-force measurements. In this setup, the smoke machine creates a layer of smoke that moves with the flow over the wing, and is illuminated by a laser sheet. Then, using a high-speed camera, we obtain a qualitative picture of the flow field around one section of the wing. We perform this two-dimensional flow visualization over three different sections along the span of the wing. Figure 9 shows a schematic of the flow visualization setup, which consists of (a) a metallic support frame, which also protects the flow from ambient disturbances (its sides are covered using a black background, and the rest is open); (b) a smoke generator, which allows control of the intensity and speed of the smoke (for the current test, it is set at the slowest swap, so that it would not spoil the hovering configuration); (c) a nozzle attached to the smoke generator, which turns the generated smoke flow into a vertical plane to cover a two-dimensional plane over a specified wing section; (d) a laser beam with lens which turns it into a plane; (e) a high-speed camera; (f) a control panel, which is used to control the FWMAV's flapping frequency; and (g) a computer interface used to process the data.

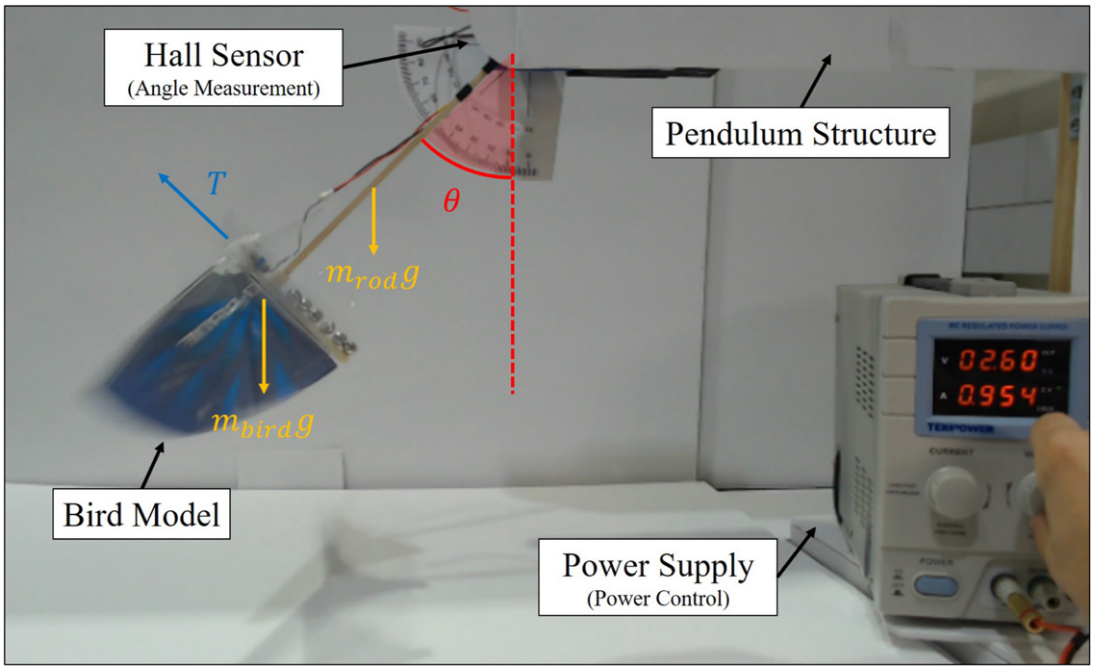

Figure 8. Average thrust and power test. The image shows the 1 DoF pendulum test with model D.

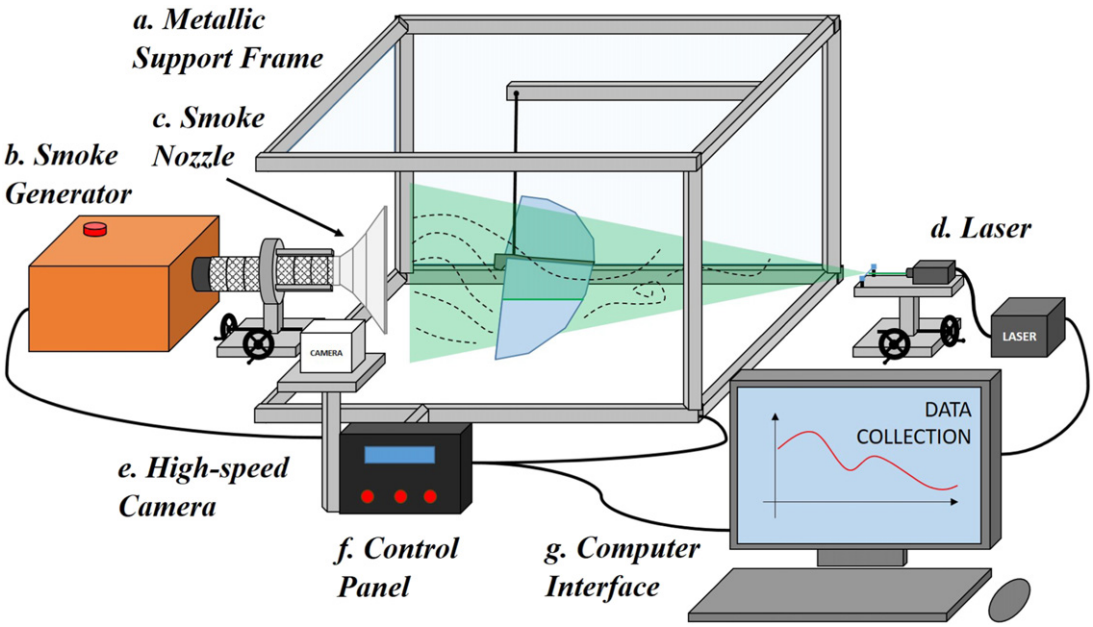

Figure 9. Flow visualization system setup. (a) Metallic support frame, (b) the smoke generator, (c) the smoke nozzle, (d) the laser, (e) the camera, (f) the control panel, and (g) the computer interface.

3. Basic force and power analysis in the absence of wing–wing interactions

Consider a wing section of width dr at a distance r from the wing root, as shown in figure 10. The differential thrust force generated on this wing section is written as

$$\mathrm{d}T(r,t) = \frac{1}{2}\rho(r\dot{\phi})^2 c(r) C_\mathrm{L}\mathrm{d}r, \tag{3}$$

where $\dot{\phi}$ is the flapping angular speed, $c(r)$ is the spanwise chord distribution, C_L is the lift coefficient, and ρ is the air density. Integrating over the wing span, we obtain

$$T(t) = \frac{1}{2}\rho\dot{\phi}^2 C_\mathrm{L}\int_0^R r^2 c(r)\mathrm{d}r. \tag{4}$$

Using the relation $\int_0^R r^2 c(r)\mathrm{d}r = SR^2\hat{r}_2{}^2$, where S is the area of one wing and $\hat{r}_2$ is the non-dimensional

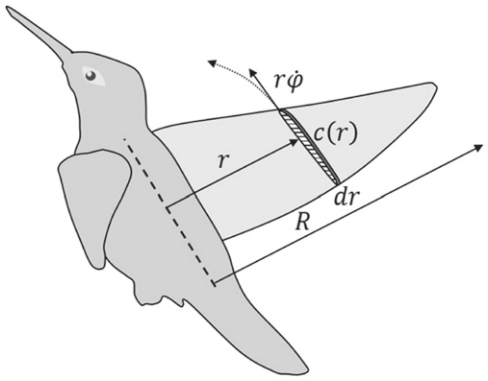

Figure 10. A schematic diagram of a flapping-wing animal.

second moment of wing area [4] and considering that $\dot{\phi} = \Phi\omega\ \sin(\omega t)$, the total thrust force by one wing is written as

$$T(t) = \frac{1}{2}\rho R^2 \Phi^2 \omega^2 S \hat{r_2}^2 C_L \sin^2(\omega t). \quad (5)$$

Ignoring the aerodynamic effects due to wing–wing interactions (e.g., clap and fling), averaging over the flapping cycle and multiplying by the number of wings, the averaged thrust generated by a multi-winged FWMAV can be written as:

$$T = N\left(\frac{1}{2}\rho V_{\text{ref}}^2 S C_{T,1}\right), \quad (6)$$

where, N is the number of wings of an FWMAV, $C_{T,1}$ is the thrust coefficient for one wing, and V_{ref} is the reference speed, which is usually taken, at hovering, as the maximum flapping speed: $V_{\text{ref}} = 2\pi f R\Phi$, where f is the flapping frequency.

If the mechanism stroke angle is the same for all FWMAV models, any particular wing in a four-wings model will sweep half the stroke angle that is swept by its peer in a two-wings configuration (see figure 11). Hence, since the above simple analysis shows that the total thrust force varies linearly with the number of wings N and quadratically with the stroke amplitude Φ, then, it implies that the thrust force $T_{4,\Phi}$ generated from a four-wings model will be half that generated by a two-wings model, driven by the same mechanism at the same frequency: $\frac{T_{4,\Phi}}{T_{2,2\Phi}} = \frac{1}{2}$ if wings interactions are ignored.

Similarly, the differential drag force on the wing section is written as

$$\mathrm{d}D(r,t) = \frac{1}{2}\rho(r\dot{\phi})^2\, c(r) C_D\, \mathrm{d}r, \quad (7)$$

where C_D is the drag coefficient. The aerodynamic power consumed by this airfoil section is then written as $\mathrm{d}P(r,t) = r\dot{\phi}\,\mathrm{d}D(r,t)$. Hence, the total power consumed by one wing is given by

$$P(t) = \frac{1}{2}\rho\dot{\phi}^3 C_D \int_0^R r^3 c(r)\mathrm{d}r \quad (8)$$

which results in

$$P(t) = \frac{1}{2}\rho R^3 \Phi^3 \omega^3 S \hat{r_3}^3 C_D \sin^2(\omega t)\sin(\omega t), \quad (9)$$

where $\hat{r_3}$ is defined as $\int_0^R r^3\, c(r)\mathrm{d}r = SR^3\hat{r_3}^3$. As such, the power consumed by a multi-winged FWMAV, ignoring wings interactions, is written as:

$$P = N\left(\frac{1}{2}\rho V_{\text{ref}}^3 S C_{P,1}\right), \quad (10)$$

where $C_{P,1}$ is the power coefficient of one wing. This aerodynamic power varies linearly with the number N of wings and cubicly with the stroke angle Φ, which implies that aerodynamic power by a four-wings model, each sweeping a stroke angle Φ, would be one-fourth of a two-wings model, each sweeping 2Φ.

In conclusion, the above analysis implies that a two-wings model, each sweeping a stroke angle 2Φ, would produce double the thrust, but consumes four times the aerodynamic power of a four-wings-model, driven by the same flapping mechanism (i.e., each wing sweeps Φ), if wing interactions are ignored. Moreover, both model types would have the same efficiency $\eta = \frac{TV_{\text{ref}}}{P} = \frac{C_{T,1}}{C_{P,1}}$, which is equal to the efficiency of one individual wing. However, these results were found to be contrary to our experimental measurements, as shown below mainly due to the effects of wing interactions.

4. Averaged thrust and power measurements

Figure 12 shows the variations of the measured thrust and aerodynamic power consumption with flapping frequency for all of the four FWMAV models described earlier. In order to extract the aerodynamic power from the total power measurements, we perform the test without the wings being installed to obtain an estimate for the mechanical power (used to drive the flapping wing mechanism); subtracting it from the total power, we managed to determine the aerodynamic power consumption. Note that the wing is extremely light in comparison to the flapping mechanism, as it is an EPP film (expanded polypropylene). So, it is expected that most of the inertial/mechanical power is spent in the mechanism, and hence, is captured by just removing the wing from the test. We show these measurement of the total power and mechanical/inertial power in the appendix and the aerodynamic power in figure 12(b).

The measured thrust and aerodynamic power consumption confirm the well-known behaviors of quadratic thrust–frequency variation and cubic power–frequency variation as shown in equations (6) and (10). Moreover table 2 shows the results of the regression equations calculated for the models A & D, which fit the experimental data almost perfectly.

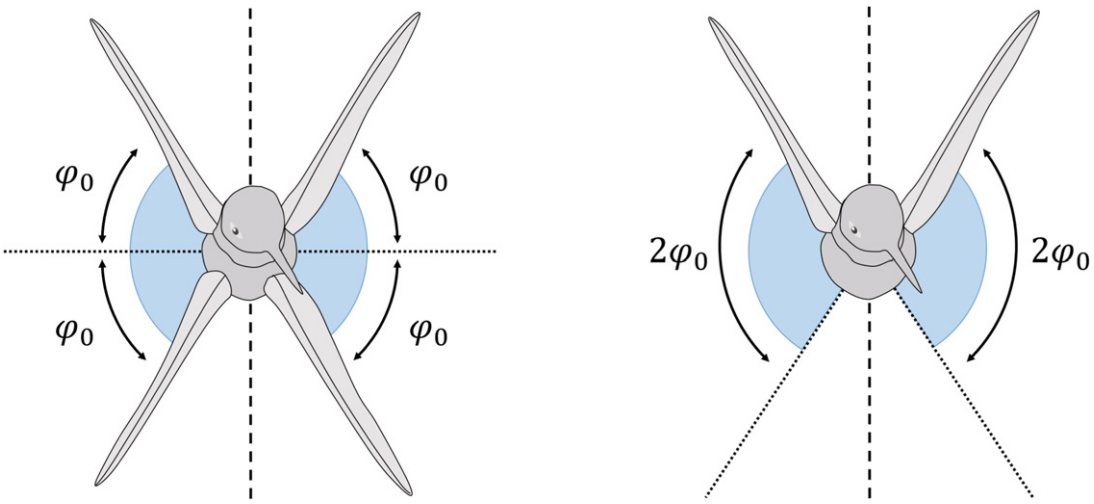

Figure 11. Angle swept by an individual wing depending on the number of wings from the FWMAV model. (a) FWMAV with four wings (model A). (b) FWMAV with two wings (model D).

However, at high frequency span-wise elastic effects led to a decrease in the angle of attack; and the thrust generation deviates from quadratic behavior, in accordance with the results of Percin *et al* [35], as seen in figure 12(a).

In contrast to the basic force and power analysis provided in section 3, ignoring wings interactions, figure 12(a) shows that the thrust of the four-wings model (model A) is significantly (almost double) higher than that of the two-wings model (model D) (this enhancement was observed to be 25% by Marden *et al* [41], two times more by Nakata *et al* [20] and Tay *et al* [31], and 44.82% by Nguyen *et al* [43]). Moreover, this significant additional thrust is generated in a considerably efficient way, for the model A requires much less power than the model D, making it almost twice efficient. Indeed, figure 12 shows that model A (four wings that clap completely) produces the largest thrust among the four models, and even consumes the least aerodynamic power, making it the most efficient among the considered four models.

To assess whether the enhanced thrust and efficiency of the four-wings model (model A) beyond the two-wings model (model D) is due to clapping, we designed two different models (B and C) with different levels of wings interactions. Both models are driven by the same mechanism as model A. The only difference is that the wings of model B would not touch each other (i.e., do not clap) if they were rigid, since there is a 23° geometrical separation between the two wings on the same side. Yet, the wings come to touch each other due to flexibility, though do not clap completely as in model A due to the geometrical separation. In contrast, the model C has a structure separator that actually prevents the wings from exceeding the designed stroke angle by virtue of their flexibility, and hence precludes any possibility of clapping. The wings of this model (C) do not clap, but enjoy some aerodynamic interactions because they come close to each other. The comparison between these two models (B and C) is quite interesting because the two mechanisms are indeed identical, and the whole models are almost identical (only one model has a structure separator, which would not be effective at all in the case of rigid wings). Despite this similarity, their aerodynamic performances are significantly different. As we can see in figure 12(a), model B produces almost 30 percent more thrust than model C when operating at the maximum frequency in the test. Moreover, their aerodynamic power consumption are quite similar, which implies that model B is significantly more efficient than model C despite the similarity. Indeed, this difference in aerodynamic performance is attributed to (partial) clapping.

Since the four models have slightly different parameters (e.g., stroke angle), we should study the normalized thrust and power. Therefore, we adopt the usual definition of thrust and power coefficients as follows:

$$C_{\mathrm{T}} = \frac{T}{N\frac{1}{2}\rho V_{\mathrm{ref}}^2 S} \tag{11}$$

$$C_{\mathrm{P}} = \frac{P}{N\frac{1}{2}\rho V_{\mathrm{ref}}^3 S}. \tag{12}$$

We also define the efficiency as $\eta = \frac{C_{\mathrm{T}}}{C_{\mathrm{P}}}$, similar to a typical hovering machine (e.g., a helicopter). It must be emphasized that this typical definition of the efficiency for a hovering mode should not be interpreted as output power relative to an input power. Figure 13 shows the variations of the thrust C_{T} and power C_{P} coefficients with the flapping frequency as well the efficiency η. Figure 13(a) shows a clear trend of thrust producing capability with clapping: C_{T} increases if more clapping is allowed, with the highest capability is observed for model A, which allows full clapping. It is also noteworthy to mention that while model C prevents clapping, it has a higher thrust producing capability than the two-wings model (D), which

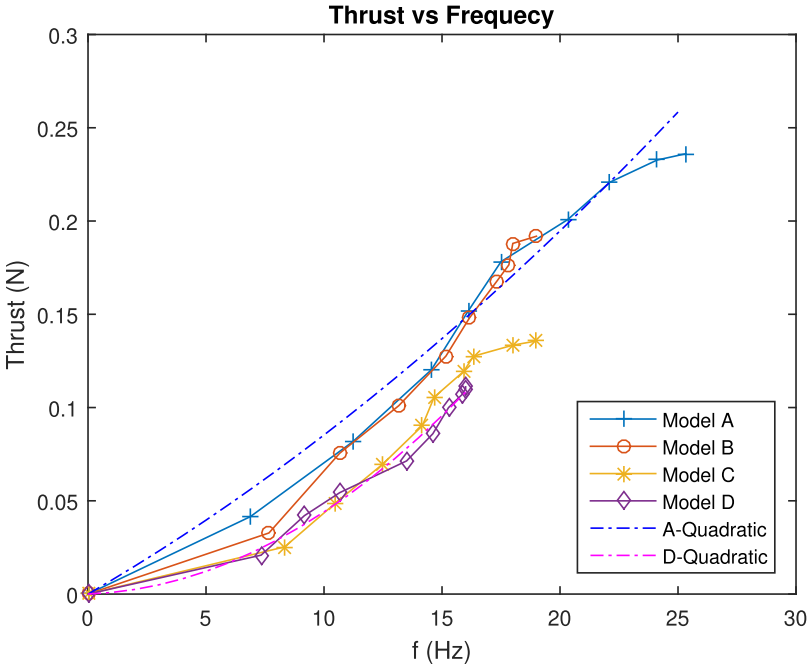

(a) Thrust vs Frequency

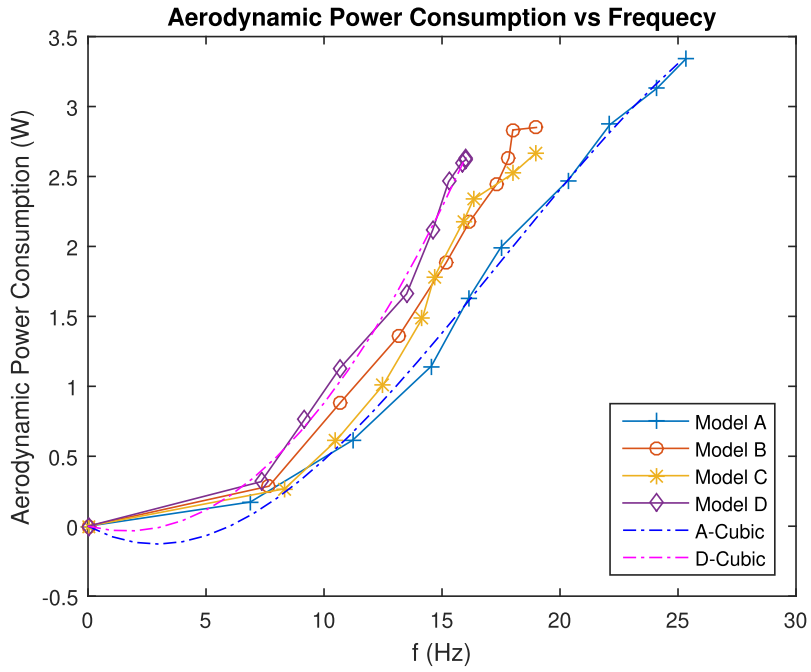

(b) Aerodynamic Power Consumption vs Frequency

Figure 12. Experimental measurements of the averaged thrust and aerodynamic power at different flapping frequencies. (a) Thrust vs frequency. (b) Aerodynamic power consumption vs frequency.

is attributed to wing–wing interactions: although the wings do not touch, they come close to each other.

As for power consumption (efficiency), model A which allows full clapping is much more efficient than the rest, with model C being the least efficient. It is interesting to conclude that an FWMAV with two wings is around two times more efficient than an FWMAV with four wings that do not clap. Indeed, clapping can be a key in the success of these FWMAVs; if sufficiently exploited, it would provide quite an efficient means of producing a significantly larger thrust than the rest of configurations that do not enjoy the same level of clapping. These results support and provide more specific quantitative values to the previous studies in literature [36, 37].

It is interesting to observe that the thrust coefficient C_T of the two-wings model (D) is almost independent of the frequency, which follows theoretical

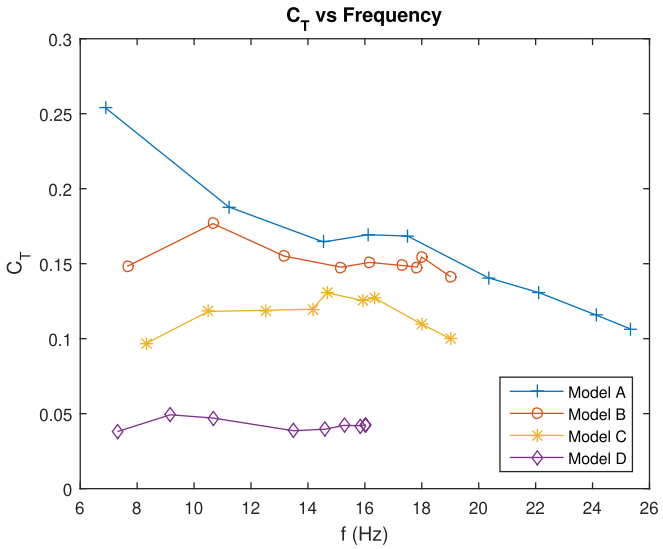

(a) C_T vs Frequency

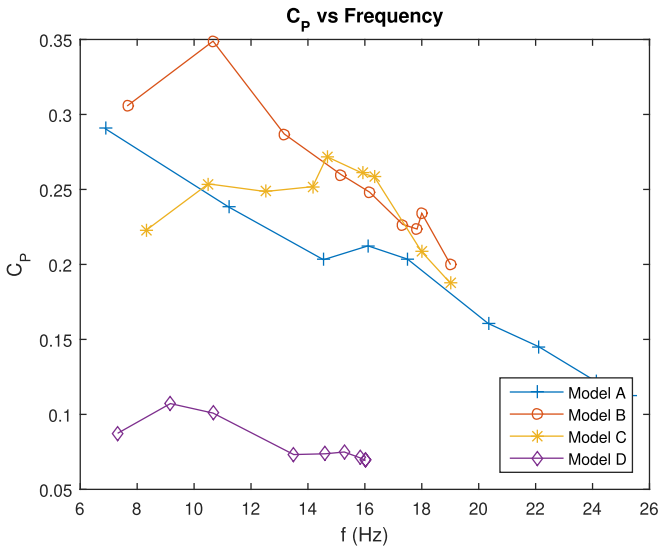

(b) C_P vs Frequency (only from the mechanism)

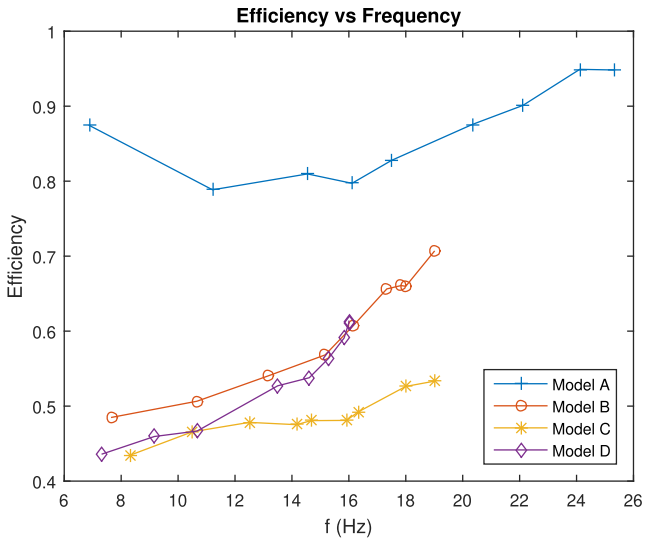

(c) Efficiency vs Frequency

Figure 13. Variations of the thrust and power coefficients C_T, C_P with frequency, as well as the efficiency $\eta = \frac{C_T}{C_P}$. (a) C_T vs frequency. (b) C_P vs frequency (only from the mechanism). (c) Efficiency vs frequency.

Table 2. Information about the multiple regressions of the models.

Plot	Model	R^2	Equation
Thrust–Freq.	A	0.980	$T(f) = 0.007\,324f + 0.000\,1205f^2$
Thrust–Freq.	D	0.990	$T(f) = 0.000\,4643f + 0.000\,394f^2$
Aero. Cons.–Freq.	A	0.996	$P(f) = -0.090\,96f + 0.017\,111f^2 - 0.000\,3272f^3$
Aero. Cons. –Freq.	D	0.995	$P(f) = -0.042\,85f + 0.013\,27f^2 - 1.84 \times 10^{-5}f^3$

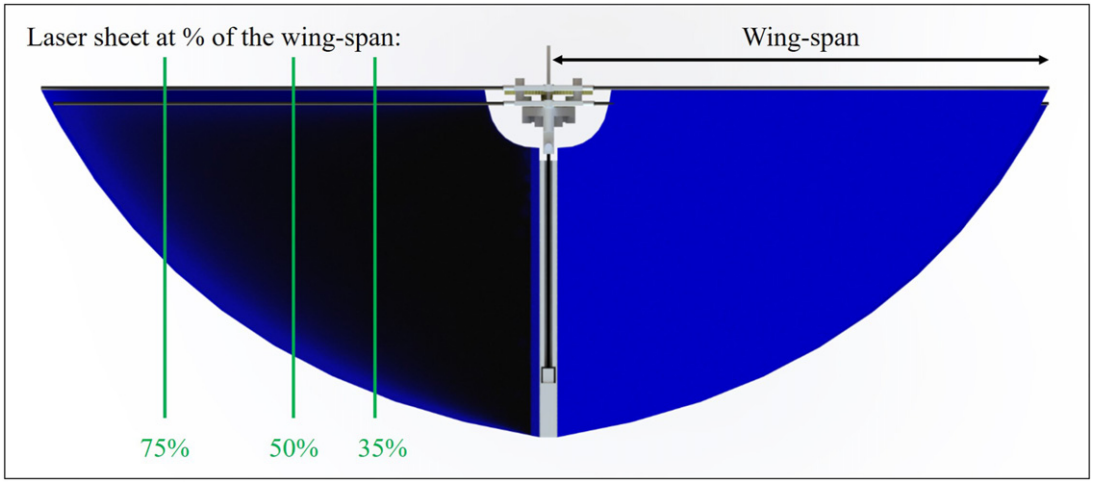

Figure 14. Schematic diagram showing the sections on the wing where the flow visualization experiment was carried out.

prediction, though its C_P experiences some variations. On the other end, it is clear that the clapping thrust enhancement effects decrease as the frequency increases as observed by Percin *et al* [35]; the less clapping effects, the less variations of C_T with frequency. It is also noteworthy to point to the maximum frequency of the system for a given drive motor. We can see how the length (stroke) of the trajectory of the wing during the cycle has an important effect on the maximum achievable frequency. Flapping with more wings that move a shorter stroke increase the maximum frequency. This result supports the recommendation of having four wings instead of two for future designs of MAV.

Finally, it is worth discussing the regression data of table 2, which shows that although both model A & D have quadratic fit for the variation of the average thrust with the flapping frequency. Model A, fitting is given by $T(f) = A_4 f + B_4 f^2$; and model D, fitting is $T(f) = A_2 f + B_2 f^2$, where $A_4 = 0.007\,324$, $B_4 = 0.000\,1205$, $A_2 = 0.000\,4643$ & $B_2 = 0.000\,394$. The coefficients of f^0 are zero because the models do not generate thrust when they are not flapping. Inspecting the coefficients of these fitting quadratic polynomials, it is interesting to observe that, $B_2 \sim 3B_4$ but, $A_4 \sim 15A_2$. Note that in the absence of wing–wing interactions, no linear dependence of average thrust on frequency is expected (only quadratic). Therefore, the fact that $B_2 > B_4$ is anticipated from the basic force analysis performed in section 3; i.e., if the effects of wing–wing interactions are neglected, then the two-wings model (D) will produce larger thrust than the four-wings model (A). Hence, the observed stark difference in linear dependence to the advantage of model A is intuitively attributed to clapping. Moreover, normalizing the thrust force to obtain the thrust coefficient (i.e., dividing by f^2), the weak linear dependence term A_2 can be neglected, resulting in an almost constant thrust coefficient for model D. In contrast, the strong linear dependence term A_4 (due to clapping) leads to a thrust coefficient that is decreasing when f is increased: the coefficient of thrust takes the form $C_T = b_4 + \frac{a_4}{f}$, where a_4 & b_4 are constants. In other words, the thrust due to clapping is dominantly linear in frequency and hence, its coefficient decreases with increasing the frequency f as observed by Percin *et al* [35].

It should be noted that while all four models have the same wing material, geometry, and kinematics (so the same aeroelastic effects) and although the only difference is the level of wing–wing interactions, the final results cannot be solely attributed to wing–wing interaction effects (e.g., clapping). These effects are enabled by specific aeroelastic properties of the wings, which are not studied in the current paper, and should be studied in the future for a more comprehensive conclusion. For example, Ramananarivo *et al* (2011) and Wu *et al* (2011) observed how flexible wings store and releases elastic energy every cycle which consequently increases its efficiency [36, 37]. Also

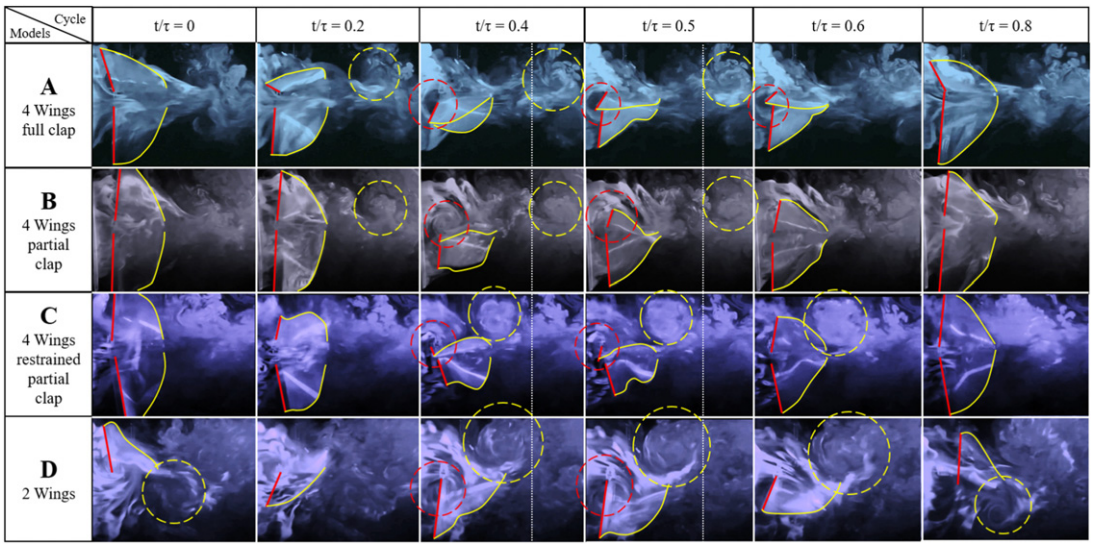

Figure 15. Flow visualization of the four different models at 35% wingspan at different time instants ($t/\tau = 0, 0.2, 0.4, 0.5, 0.6$ & 0.8) during a cycle. The red bold line represents a wing leading edge (LE), the yellow bold line represents a wing TE, the red dashed line circumscribes an LEV and the yellow dashed line circumscribes a TEV.

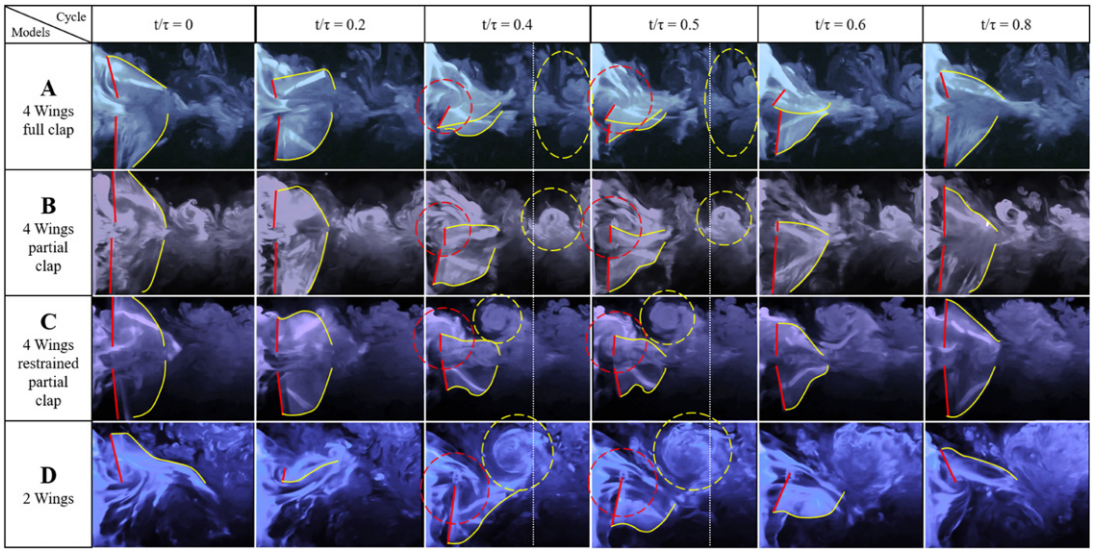

Figure 16. Flow visualization of the four different models at 50% wingspan at different time instants ($t/\tau = 0, 0.2, 0.4, 0.5, 0.6$ & 0.8) during a cycle. The red bold line represents a wing LE, the yellow bold line represents a wing TE, the red dashed line circumscribes an LEV and the yellow dashed line circumscribes a TEV.

Kim *et al* (2013) showed how different aspect ratios and stroke angles of clapping motion have effect on the generation of thrust [38]. We also observed a similar effect: decreasing the size of the wing by half reduced the efficiency significantly at the same range of frequencies (almost 50%) [49].

The averaged thrust and power measurements, discussed above, imply that clapping indeed provides a significantly efficient thrust enhancement. It is interesting to study the underlying physics behind such a thrust enhancement mechanism, which is attempted in the next section using flow visualization.

5. Flow visualization

The two-dimensional flow visualization experiment, discussed in section 2.3, was carried out at three different parallel sections along the span of the wing. These sections are shown schematically in figure 14. For each of the four FWMAV models, a qualitative flow field at 35% and 50% of the wing-span are shown in figures 15 and 16. There is no free stream considered for these cases (i.e., pure hovering). The comparison was made for the different FWMAV models flapping at the same frequency. The flow was captured

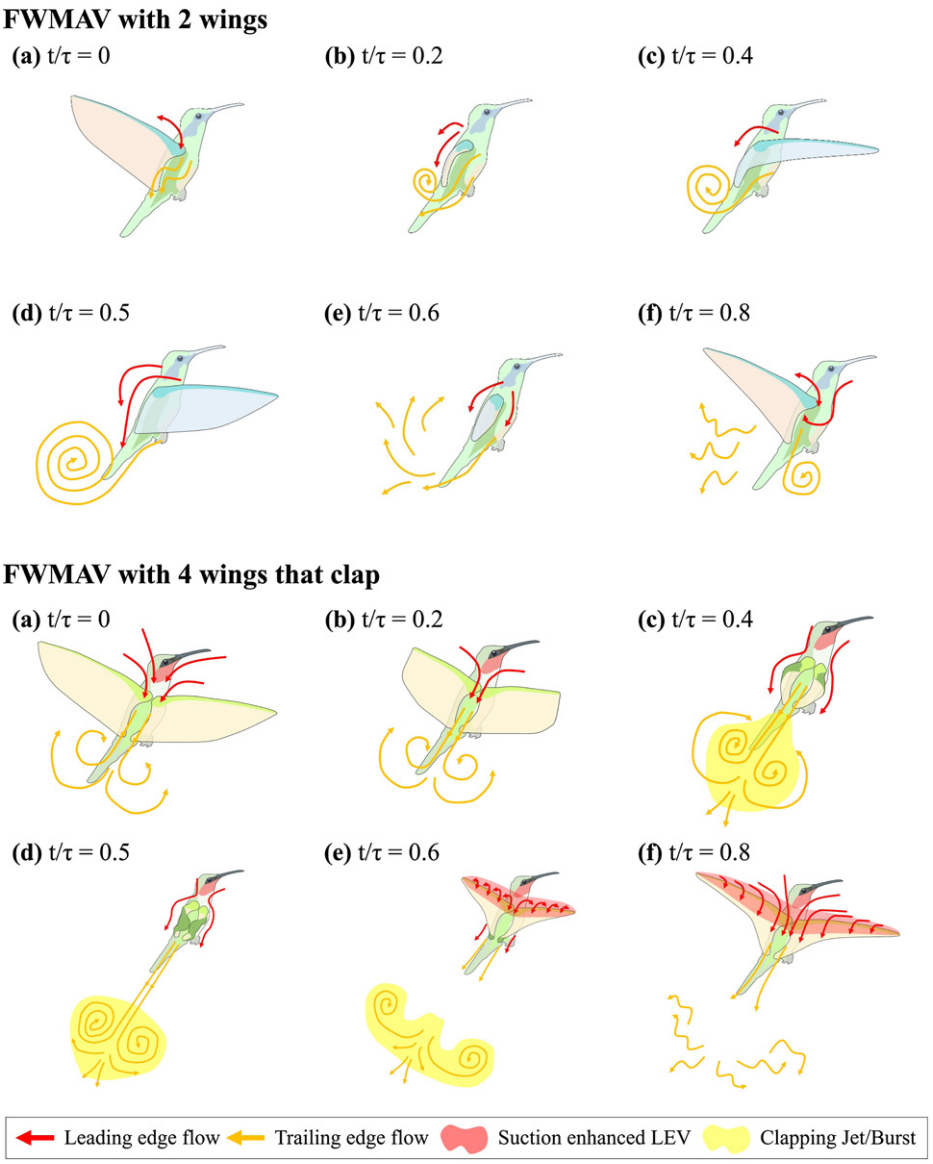

Figure 17. A schematic comparing the flow fields over a clapping four-wing FWMAV model and a non-clapping two-wing FWMAV model. (a) Stroke start: no appreciable LE flow over the two-wing FWMAV model while the opening of the clapping wings creates a suction of the flow near the LE inside the space between the wings. (b) Middle of downstroke: in both cases, the wings attain maximum translational speed and a TEV is formed. However, in the clapping case, there are two counter-rotating TEVs (one per each wing), which increases the downstream flow in the opening space between the wings. (c) and (d) End of downstroke and beginning of upstroke: in both cases, the wings come to a stop and the TEVs become larger. In four-wings model, the wings are completely closed, ejecting downstream the sucked air between the wings in the form of a jet (air burst), which washes away the TEVs. (e) Middle of upstroke: the TEVs are further away from wings in the clapping case whereas the TEV, in the two-wings model, has diffused.

at six different instants ($t/\tau = 0$, 0.2, 0.4, 0.5, 0.6 & 0.8) during the cycle, where $\tau = 1/f$ is the flapping period.

Figure 15 shows a clear difference between the flow fields of models A and D. Perhaps, the only similarity that can be observed is the presence of a LEV (circumscribed by red dashed circle). However, the figure shows that the lifting mechanism in models A and D are fundamentally different. For model A, during the first half of the cycle where the wings are opening up (departing from each other or during 'fling'), the air is sucked in the open space between the wings, and when the wings are closing the air mass accumulated during the previous half-stroke is forcibly ejected downstream (in accordance with Sane's observation [30]). That is, the clapping model (A) enjoys a jet-effect thrusting mechanism—we call it a *thrust burst*. Similar behavior is observed for model B. In contrast, the two wings model (D) experiences a classical unsteady lifting mechanism: a trailing edge vortex (TEV) (*starting vortex*) is shed whenever there is a change in the wing motion which, by virtue of conversation of circulation, leads to a change in the wing bound circulation (and consequently lift). This unsteady lifting mechanism has a transient response (Wagner's response [50]) due to such a TEV [30]; the closer the TEV to the wing, the smaller the unsteady lift in comparison to the steady value corresponding

to the instantaneous wing motion. Therefore, insofar as the starting TEV is essential to the lift development because it dictates how much circulation around the wing, it is negatively impacting the transient lift development; the steady lift is not attained until the starting TEV is washed away. It is interesting to observe that the bursting jet in the clapping models (A and B) washes away the TEV [44]; it convects downstream much faster than in the case of model D, as shown in figure 15 and the explanatory schematic in figure 17. Also, in the four-wings model, there are two counter-rotating TEVs per side (one per wing). As traditionally known, these counter-rotating vortices induce a downstream flow on each other [28], increasing their convective speed even more. As a result, the TEVs are always further away from the wings in A, B than in D.

In the case of model C, which has a separator that restrains clapping, figure 15 shows that the air sucked in the opening phase is not strongly ejected in the form of a jet; the separator precludes the wings from closing and compressing the accumulated air mass between them to form a jet. Moreover, the figure also shows a TEV close to the trailing edge (TE) in this case. It can be recognized comparatively that the location of the TEV is furthest downstream for models A & B, but near the TE for models C & D. This explains why models A & B have more thrust than models C & D. But, to understand the difference between models A & B, we need to look into the flow visualization at 50% wingspan which is shown in figure 16.

The wing translational speed ($r\dot{\varphi}$) at 50% of the wingspan is larger than at 35%, leading to larger convective speeds and stronger effects. For example the bursting jets are clearer in figure 16 than in figure 15. Additionally, figure 16 shows a LEV in all models at the instances $t/\tau = 0.4$ & 0.5. In the non-clapping models C and D, the TEVs are close to TE of the wings, with the TEV in model C being little further off from the TE than in model D. For models A & B, the figure shows that the air is sucked in the early instances of the flapping cycles and is ejected downstream in the form of a jet as observed by Sane [30] and Jadhav [29]. Similar to the 35% flow, figure 16 shows TEVs in the clapping models A and B further away from the wings than in the non-clapping models C and D. Finally, to better present the main flow features, a schematic in figure 16 provides a qualitative comparison between the flow field of model A and that of model D.

6. Conclusion

In this paper, we developed four models of bio-inspired flying robots with different levels of wing clapping: model (A) with four wings that completely clap, model (B) with four wings that partially clap, model (C) with four wings that do not clap but enjoy some wing–wing interactions, and model (D) with two wings (no clapping or wing–wing interactions). The aerodynamic performance of the four models was tested in terms of the averaged thrust and power consumption at various flapping frequencies. The four models are driven by the same flapping mechanism, which implies that each wing in the two-wings model sweeps double the stroke angle of a wing in the four-wings model. The study showed that the more clapping, the more thrust at the same frequency; the full clapping model (A) produces the largest thrust at a given flapping frequency. Moreover, it even consumes the lowest power, making it the most efficient among the four models. That is, an air vehicle with four wings that clap is significantly more efficient (almost double) and generates more thrust than the same air vehicle with only two wings sweeping double the stroke. Furthermore, from a mechanical perspective, flapping along a shorter stroke allows operating at higher frequencies. In this regard, the four-wings model will be to operate at higher frequencies, hence generating more thrust than a two-wings model. To better understand the underlying physics behind this enhanced thrust capability due to clapping, we performed flow visualization around the flapping wings of the four models at different instants during the flapping cycle. The flow visualization study revealed that, during the opening phase of the wings in a clapping model, an air mass is sucked in the open area between the wings. As the wings close, this air mass is ejected in the form a jet, creating an additional thrust. Moreover, this jet washes away the vortices shed from the TEs, thereby diminishing their adverse transient effects on the wing lift development. In contrast, the two-wings model do not enjoy such a jet effect and its TE vortices convect at a smaller speed. Hence, they stay in close proximity to the wing during some part of the cycle, negatively impacting its transient lift development. The presented flow visualization showed that the more clapping, the stronger the jet, and the further the TE vortices are away from the wing.

Acknowledgments

The authors would like to acknowledge the work from Wai Hnin Oo, Johnson Ly, Charline Petit and Thomas Naess, who helped in the building of the models, and their average thrust and power testing. Additionally, the authors appreciate the support from Alexander Lopez, Kevin Huang and Fernando Pablo Quevedo, who helped in the building of the flow visualization setup, and the testing using the slow motion capture system. Finally, the project received funding from the NSF Grant CMMI-1846308, and the Balsells Fellowship Foundation.

Data availability statement

The data that support the findings of this study are available upon reasonable request from the authors.

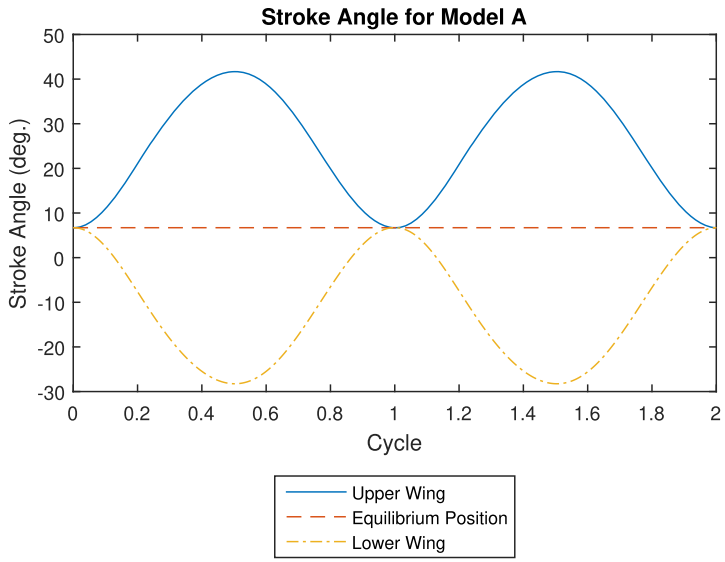

(a) Stroke Angle from the mechanism of Model A

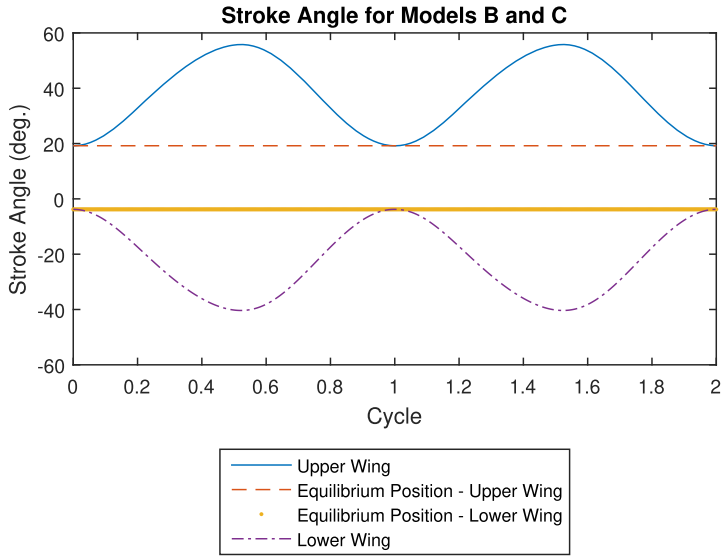

(b) Stroke Angle from the mechanism of Models B and C

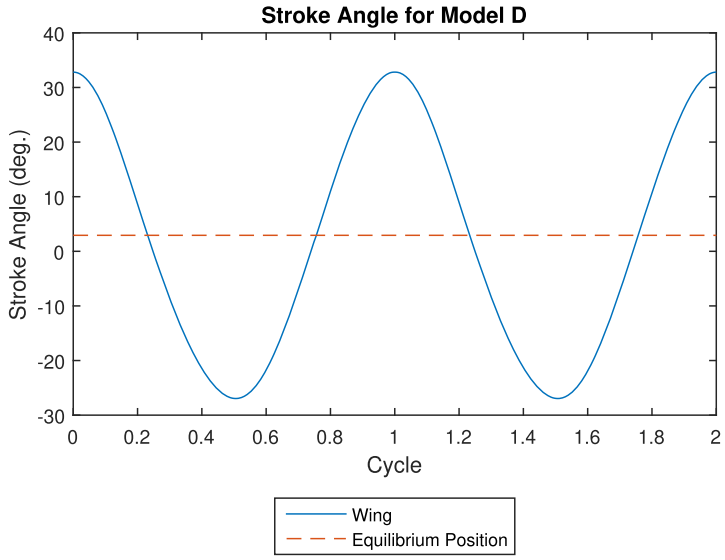

(c) Stroke Angle from the mechanism of Model D

Figure A1. Stroke angles from crank rocker mechanism of each model. (a) Stroke angle from the mechanism of model A. (b) Stroke angle from the mechanism of models B and C. (c) Stroke angle from the mechanism of model D.

Table A1. Stroke angle and crank rocker linkage ratios.

FWMAV	Stroke angle	Position of the wing/s	*r*2/*r*1	*r*3/*r*1	*r*4/*r*1
Model A	35°/wing	0° to ±35°	0.178	0.797	0.59
Models B & C	37°/wing	±11.5° to ±48.5°	0.162	0.726	0.54
Model D	60°/wing	−35°–35°	0.178	0.92	0.36

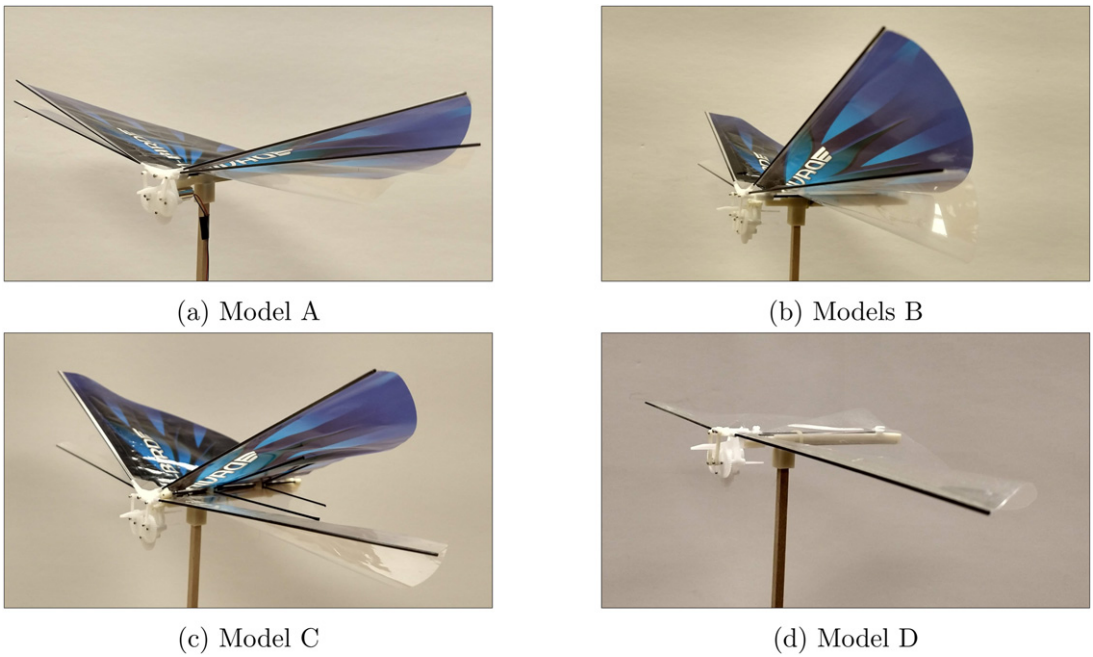

Figure A2. Top-left corner view of the real models used in the research. (a) Model A. (b) Model B. (c) Model C. (d) Model D.

Appendix A. Experimental setup

A.1. Characterization of the models

There are a couple points that can be explained further in order to understand better the models used in our research. The first is the type of mechanism used to generate the dynamics of the wings. The crank rocker mechanism is a four bar linkage that transforms a rotational motion into oscillatory. This mechanism uses four bars with different lengths, in where the shortest one (bar 2) rotates while the opposite linkage (bar 4) oscillates. The other two bars usually are longer and they are calculated to provide the required oscillatory motion. The equations that govern the relations between the bars are explained in previous publications of our research [24].

In figure 7(a), we can see the schematic of the crank rocker mechanism. It shows the bars from the crank rocker mechanism and how they are applied in to the passive mechanism. Figure 7(b) shows the crank rocker applied in model A, which is the FWMAV that uses only two wings to fly.

The mechanisms have been designed for an specific stroke angles, such that they provide the optimized dynamics for the wings. The way used to achieve these angles has been by adjusting the relation between the bars, using the equations that we mentioned previously. In general, these dynamics are obtained by selecting the right ratios, which are the result of defining the stroke angle of the wings and the minimum angle between the linkages. Then, the lengths of the linkages can be obtained by selecting the length of bar 1, and multiplying it with the ratios. The ratios we used in our mechanisms are shown in table A1.

The crank rocker ratios, the stroke angles and the position of the wing/s for each mechanism are in figure A1. The plots show both the stroke angle of the wings as well as the equilibrium position of them. These are result of the motion of bar four plus the extension (see figure 7(b)). In figure A1(a), which is model D, the wing travels around 60° in where the equilibrium is almost in 0°. This helps the mechanism to be more balanced during the flight as the wings move more symmetrically with respect to the front and the back of the FWMAV. Model A has a similar performance but it divides the path by two, half per each wing (35° each wing). As we can see in figure A1(c), despite each wing travels less, the combined stroke angle is 70°, which is 10 more° than model A. Additionally, the equilibrium point is quite close to 0°, making this FWMAV also balanced.

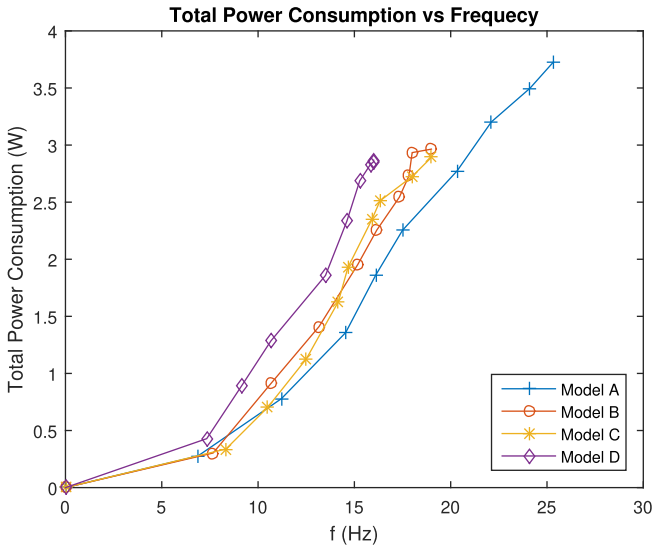

(a) Total Power Consumption vs Frequency

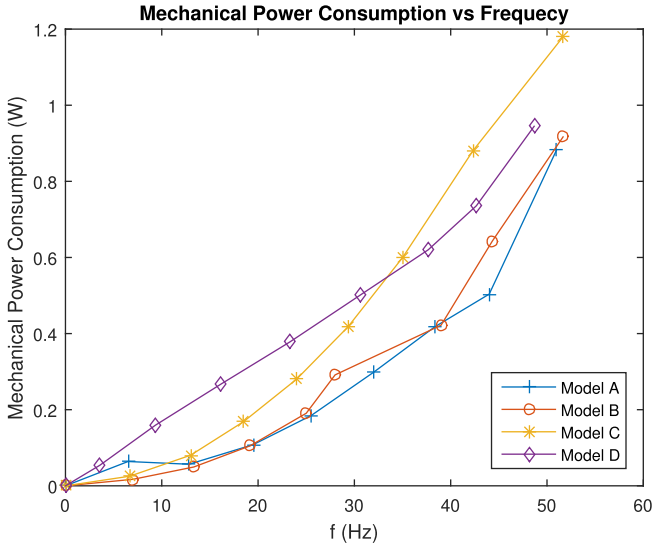

(b) Mechanical Power Consumption vs Frequency

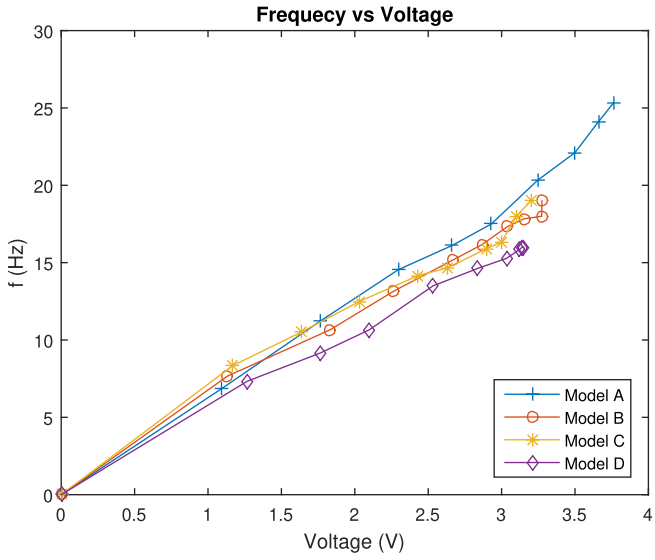

(c) Frequency vs Voltage

Figure B1. Additional results from the average thrust and power test. (a) Total power consumption vs frequency. (b) Mechanical power consumption vs frequency. (c) Frequency vs voltage.

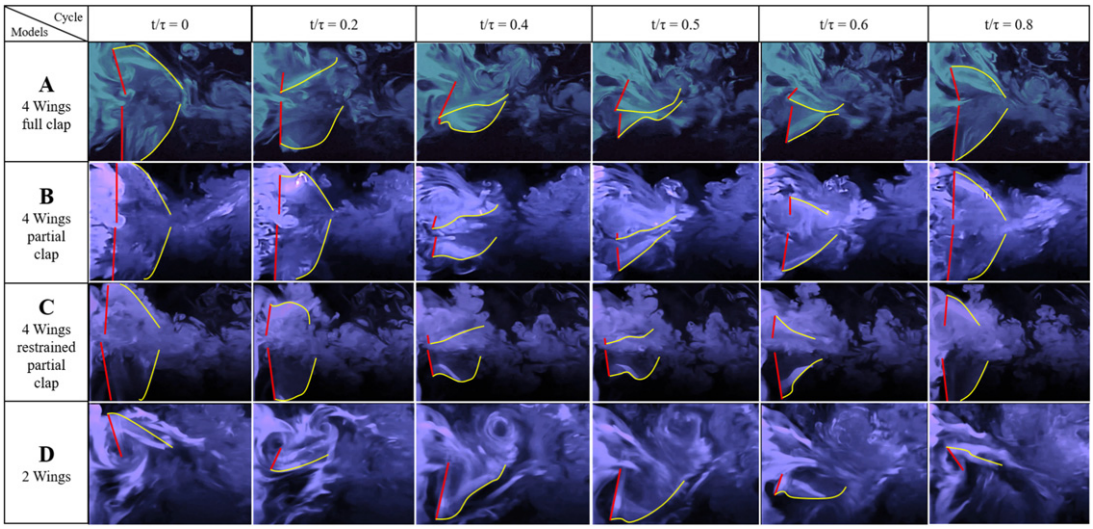

Figure B2. Flow visualization of the four different FWMAVs at 75% wingspan showing different time snaps ($t/\tau = 0$, 0.2, 0.4, 0.5, 0.6 & 0.8) during a cycle where the four models are (1) four wings full clap, (2) four wings partial clap, (3) four wings restrained partial clap (4) two wings.

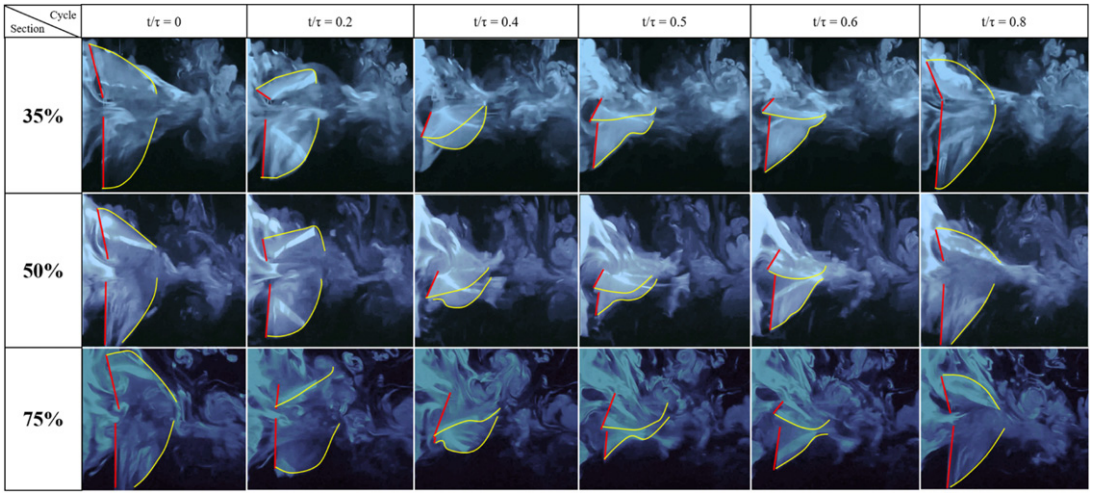

Figure C1. Flow visualization from model A. Flow captured at 35%, 50% and 75% of the wingspan.

On the other hand, there are the dynamics from models B and C, which are shown in figure A1(b). They are very similar to model D, being the combined stroke angle of both wings 74°. However, in order to achieve that behavior without closing the wings completely, it was necessary to sacrifice part of the balance from the mechanism. As you can see, the average equilibrium would be around 8°, which makes the equilibrium from each wing at −2° and 20°. This creates some of vibrations into the system, that luckily end up no affecting the consumption and performance. Of course, this would have brought critical issues if the model was flying alone instead of being attached to a pendulum. Even a little vibration would have compromised the stability of the system.

Finally, the FWMAVs are made out of injected plastic except for the pieces that were modified, that are 3D printed using a modified-ABS (see figure A2). Additionally, all FWMAVs are powered all using a 19.5 kV DC motor, and have flexible and very light wings.

Appendix B. Averaged thrust and power measurements

There are some additional plots from the 'average thrust and power test' that can validate even more this study. First of all, there is the total power consumption vs frequency (see figure B1(a)), and the mechanical power consumption vs frequency (see figure B1(a)). Although these plots are introduced and explained in the paper, it is now visible how different is the magnitude of their units. That is the main reason why the aerodynamical power consumption is very close the total. Finally, the performance from each mechanism depends completely on its design and

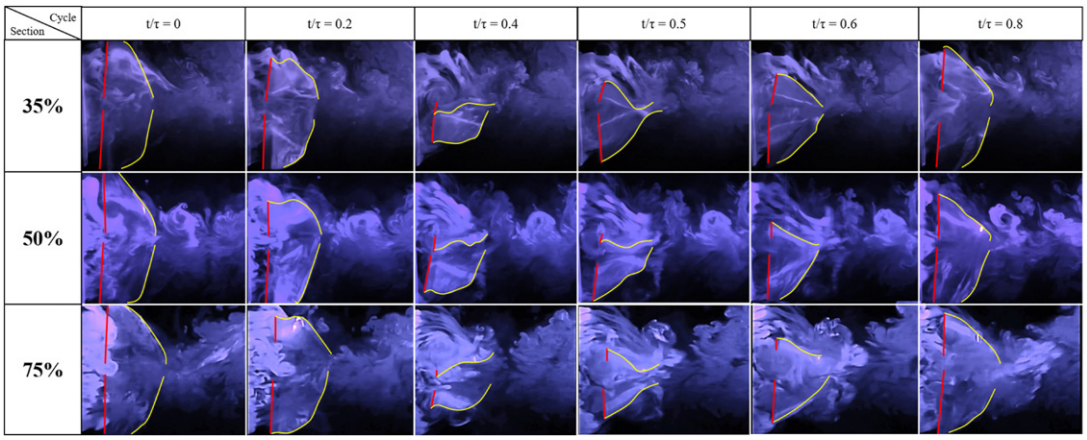

Figure C2. Flow visualization from model B. Flow captured at 35%, 50% and 75% of the wingspan.

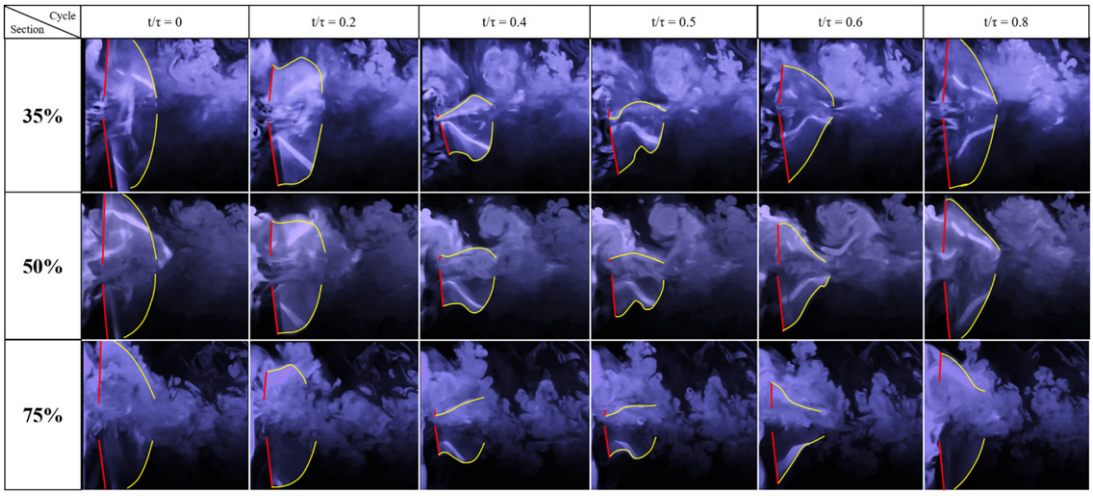

Figure C3. Flow visualization from model C. Flow captured at 35%, 50% and 75% of the wingspan.

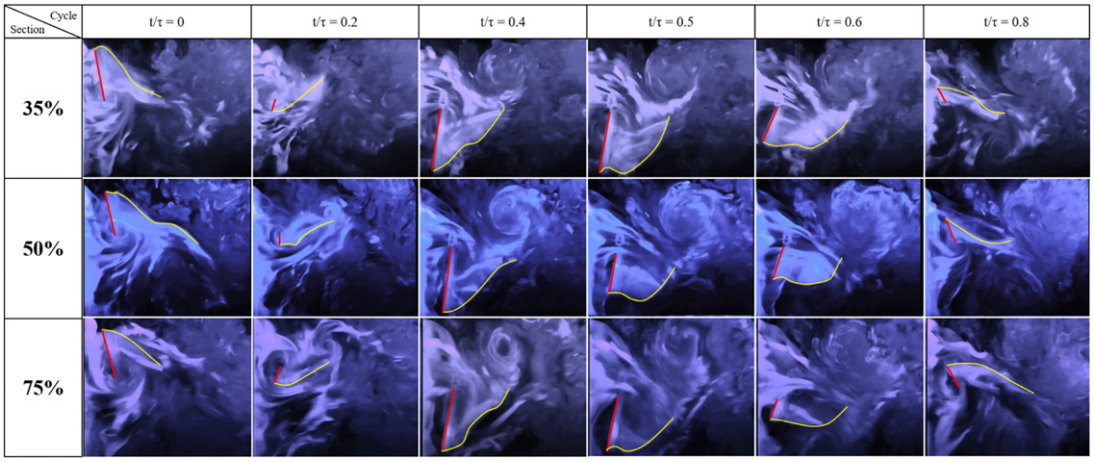

Figure C4. Flow visualization from model D. Flow captured at 35%, 50% and 75% of the wingspan.

the manufacturing procedure. Consequently, model A is the one that consumes less energy as its crank rocker configuration and manufacturing procedure (outside purchase) are the most optimal.

On the other hand, the relation between the voltage and the frequency has been a crucial to control the models. Figure B1(c) shows this relation, in where the voltage is proportional to the frequency. The only difference is the maximum voltage per model, which is directly related to the maximum thrust that can be generated by that model.

Table 2 shows the results of the regression equations calculated for the models A and D, which fit the experimental data almost perfectly.

Appendix C. Flow visualization

Figure B2 compares the flow field for all the FWMAVs at 75% of the wing-span. It can be seen that apart from model D, everywhere the flow is turbulent in all the phases. At this section the velocity of flapping is much higher and probably that is why the vortices dissipate much faster compared to the sections mentioned before.

C.1. Three dimensional visualization of individual models

There are some additional flow visualization comparison has been done on those four models. Figures C1, C2, C3 and C4 are looking into the flow field from a different view point. The comparison in these figures are made for a single model but for different sections of the wing. It is clear in figure C4 that in the phases of $t/\tau = 0.4$ & 0.5 the TE vortices are becoming more and more prominent closer to the tip of the wing. In figure C1 also the difference in relative positions of the TE vortices can be seen for different sections. Same can be said for figures C2 and C3.

ORCID iDs

Miquel Balta https://orcid.org/0000-0001-5152-059X

References

[1] Pines D J and Algeria T (Defense Advanced Research Projects Agency) 2005 *Nano Air Vehicle (Nav) Program* https://www.federalgrants.com/Nano-Air-Vehicle-Nav-Program-1297.html (Accessed 01 09 2017)
[2] Hassanalian M and Abdelkefi A 2017 Classifications, applications, and design challenges of drones: a review *Prog. Aerosp. Sci.* **91** 99–131
[3] Todd H, Martin C, Tun R and Castelli V 2012 The DARPA nano air vehicle program *50th AIAA Aerospace Sciences Meeting Including the New Horizons Forum and Aerospace Exposition*
[4] Ellington C P 1984 The aerodynamics of hovering insect flight: IV. Aerodynamic mechanisms *Phil. Trans. R. Soc.* B **305** 79–113
[5] Ellington C P, Van Den Berg C, Willmott A P and Thomas A L R 1996 Leading-edge vortices in insect flight *Nature* **384** 626
[6] Dickinson M H, Lehmann F-O and Sane S P 1999 Wing rotation and the aerodynamic basis of insect flight *Science* **284** 1954–60
[7] Taha H E, Tahmasian S, Woolsey C A, Nayfeh A H and Hajj M R 2015 The need for higher-order averaging in the stability analysis of hovering, flapping-wing flight *Bioinspir. Biomim.* **10** 016002
[8] Taha H E, Nayfeh A H and Hajj M R 2014 Effect of the aerodynamic-induced parametric excitation on the longitudinal stability of hovering MAVs/insects *Nonlinear Dyn.* **78** 2399–408
[9] Taha H, Kiani M and Navarro J 2017 Experimental demonstration of the vibrational stabilization phenomenon in bio-inspired flying robots *IEEE Robot. Autom. Lett.* **3** 643–7
[10] Hassan A M and Taha H E 2019 Differential-geometric-control formulation of flapping flight multi-body dynamics *J. Nonlinear Sci.* **29** 1379–417
[11] Taha H E, Kiani M, Hedrick T L and Greeter J S M 2020 Vibrational control: a hidden stabilization mechanism in insect flight *Sci. Robot.* **5** eabb1502
[12] Whitney J P 2012 Design and performance of insect-scale flapping-wing vehicles *PhD Thesis* Harvard University
[13] Keennon M, Klingebiel K and Won H 2012 Development of the nano hummingbird: a tailless flapping wing micro air vehicle *50th AIAA Aerospace Sciences Meeting Including the New Horizons Forum and Aerospace Exposition*
[14] de Croon G C H E, Groen M A, De Wagter C, Remes B, Ruijsink R and van Oudheusden B W 2012 Design, aerodynamics and autonomy of the delfly *Bioinspir. Biomim.* **7** 025003
[15] de Croon G C H E, Perçin M, Remes B, Ruijsink R and De Wagter C 2016 *The Delfly* vol 10 (Berlin: Springer) pp 978–94
[16] Doman D B, Oppenheimer M W and Sigthorsson D O 2010 Wingbeat shape modulation for flapping-wing micro-air-vehicle control during hover *J. Guid. Control Dyn.* **33** 724–39
[17] Oppenheimer M W, Doman D B and Sigthorsson D O 2011 Dynamics and control of a biomimetic vehicle using biased wingbeat forcing functions *J. Guid. Control Dyn.* **34** 204–17
[18] Schenato L, Campolo D and Sastry S 2003 Controllability issues in flapping flight for biomimetic micro aerial vehicles (MAVs) *42nd IEEE Int. Conf. Decision and Control (IEEE Cat. No. 03CH37475)* vol 6 (Piscataway, NJ: IEEE) pp 6441–7
[19] Taha H E, Nayfeh A H and Hajj M R 2013 Saturation-based actuation for flapping MAVs in hovering and forward flight *Nonlinear Dyn.* **73** 1125–38
[20] Nakata T, Liu H, Tanaka Y, Nishihashi N, Wang X and Sato A 2011 Aerodynamics of a bio-inspired flexible flapping-wing micro air vehicle *Bioinspir. Biomim.* **6** 045002
[21] Berman G J and Wang Z J 2007 Energy-minimizing kinematics in hovering insect flight *J. Fluid Mech.* **582** 153–68
[22] Yan Z, Taha H E and Hajj M R 2015 Effects of aerodynamic modeling on the optimal wing kinematics for hovering MAVs *Aerosp. Sci. Technol.* **45** 39–49
[23] Chen C and Zhang T 2019 A review of design and fabrication of the bionic flapping wing micro air vehicles *Micromachines* **10** 144
[24] Balta M, Ahmed K A, Wang P L, McCarthy J M and Taha H E 2017 Design and manufacturing of flapping wing mechanisms for micro air vehicles *58th AIAA/ASCE/AHS/ASC Structures, Structural Dynamics, and Materials Conf.*
[25] Mukikim eBird 2016 *eBird Blue [Pigeon] - x2 Channel RC Flying Bird* https://mukikim.com/shop/ols/products/ebird-blue-pigeon-x2-channel-rc-flying-bird (Accessed 01 09 2017)
[26] Weis-Fogh T 1973 Quick estimates of flight fitness in hovering animals, including novel mechanisms for lift production *J. Exp. Biol.* **59** 169–230
[27] Weis-Fogh T 1975 Unusual mechanisms for the generation of lift in flying animals *Sci. Am.* **233** 80–7
[28] Armanini S F, Caetano J V, de Croon G C H E, de Visser C C and Mulder M 2016 Quasi-steady aerodynamic model of clap-and-fling flapping MAV and validation using free-flight data *Bioinspir. Biomim.* **11** 046002
[29] Jadhav S S, Lua K B and Tay W B 2019 Effect of clap-and-fling mechanism on force generation in flapping wing micro aerial vehicles *Bioinspir. Biomim.* **14** 036006
[30] Sane S P 2003 The aerodynamics of insect flight *J. Exp. Biol.* **206** 4191–208
[31] Tay W B, van Oudheusden B W and Bijl H 2014 Numerical simulation of x-wing type biplane flapping wings in 3D using the immersed boundary method *Bioinspir. Biomim.* **9** 036001

[32] Martin N, Roh C, Idrees S and Gharib M 2017 To flap or not to flap: comparison between flapping and clapping propulsions *J. Fluid Mech.* **822** R5
[33] Miller L A and Peskin C S 2005 A computational fluid dynamics of 'clap and fling' in the smallest insects *J. Exp. Biol.* **208** 195–212
[34] Percin M, Hu Y, van Oudheusden B W, Remes B and Scarano F 2011 Wing flexibility effects in clap-and-fling *Int. J. Micro Air Veh.* **3** 217–27
[35] Percin M, van Oudheusden B W, de Croon G C H E and Remes B 2016 Force generation and wing deformation characteristics of a flapping-wing micro air vehicle 'DelFly II' in hovering flight *Bioinspir. Biomim.* **11** 036014
[36] Ramananarivo S, Godoy-Diana R and Thiria B 2011 Rather than resonance, flapping wing flyers may play on aerodynamics to improve performance *Proc. Natl Acad. Sci.* **108** 5964–9
[37] Wu P, Stanford B K, Sällström E, Ukeiley L and Ifju P G 2011 Structural dynamics and aerodynamics measurements of biologically inspired flexible flapping wings *Bioinspir. Biomim.* **6** 016009
[38] Kim D, Hussain F and Gharib M 2013 Vortex dynamics of clapping plates *J. Fluid Mech.* **714** 5–23
[39] Wakeling J and Ellington C P 1997 Dragonfly flight: I. Gliding flight and steady-state aerodynamic forces *J. Exp. Biol.* **200** 543–56
[40] Armanini S F, Caetano J V, de Visser C C and de Croon G 2017 Modelling wing wake and tail–wake interaction of a clap-and-peel flapping-wing MAV *AIAA*
[41] Marden J H 1987 Maximum lift production during takeoff in flying animals *J. Exp. Biol.* **130** 235–58
[42] Cheng X and Sun M 2017 Aerodynamic forces and flows of the full and partial clap-fling motions in insects *Life and Enviroment Sciences*
[43] Nguyen Q-V, Chan W L and Debiasi M 2014 Design, fabrication, and performance test of a hovering-based flapping-wing micro air vehicle capable of sustained and controlled flight *IMAV 2014: Int. Micro Air Vehicle Conf. Competition* (12–15 August 2014) (Delft, The Netherlands: Delft University of Technology)
[44] Lehmann F-O, Sane S P and Dickinson M 2005 The aerodynamic effects of wing–wing interaction in flapping insect wings *J. Exp. Biol.* **208** 3075–92
[45] Lehmann F-O and Pick S 2007 The aerodynamic benefit of wing–wing interaction depends on stroke trajectory in flapping insect wings *J. Exp. Biol.* **210** 1362–77
[46] Kolomenskiy D, Moffatt H K, Farge M and Schneider K 2011 The Lighthill–Weis–Fogh clap–fling–sweep mechanism revisited *J. Fluid Mech.* **676** 572–606
[47] Arora N, Gupta A, Sanghi S, Aono H and Shyy W 2014 Lift-drag and flow structures associated with the 'clap and fling' motion *Phys. Fluids* **26** 071906
[48] Wood R J 2008 The first takeoff of a biologically inspired at-scale robotic insect *IEEE Trans. Robot.* **24** 341–7
[49] Zakaria M 2021 Experimental Investigation of aerodynamic characteristics of a four-winged flapping *Master's Thesis* University of California, Irvine
[50] Wagner H 1925 Über die Entstehung des dynamischen Auftriebes von Tragflügeln *Z. Angew. Math. Mech.* **5** 17–35